

1 **Mapping the spatio-temporal distribution of key vegetation cover properties in lowland river**
2 **reaches, using digital photography**

3 **Authors:** Veerle Verschoren^{1*}, Jonas Schoelynck¹, Kerst Buis¹, Fleur Visser², Patrick Meire¹, Stijn
4 Temmerman¹

5
6 1. *University of Antwerp, Department of Biology, Ecosystem Management Research Group,*
7 *Universiteitsplein 1C, B-2610 Wilrijk, Belgium.*

8 2. *University of Worcester, Institute of Science and the Environment, Henwick Grove,*
9 *Worcester WR2 6AJ, UK*

10

11 ***Corresponding author**

12 UA - Campus Drie Eiken

13 Ecosystem Management research group

14 Universiteitsplein 1

15 Building C, C1.20

16 B - 2610 Wilrijk, Belgium

17

18 verschoren.veerle@hotmail.com

19 Tel +32 3 265 22 52

20 Fax +32 3 265 22 71

21

22 **Abstract**

23 The presence of vegetation in stream ecosystems is highly dynamic in both space and time. A
24 digital photography technique is developed to map aquatic vegetation cover at species level, which
25 has a very-high spatial and a flexible temporal resolution. A digital single-lens-reflex (DSLR)
26 camera mounted on a handheld telescopic pole is used. The low-altitude (5 m) orthogonal aerial
27 images have a low spectral resolution (Red-Green-Blue), high spatial resolution (~ 1.9 pixels cm^{-2} ,
28 ~ 1.3 cm length) and flexible temporal resolution (monthly). The method is successfully applied in
29 two lowland rivers to quantify four key properties of vegetated rivers: vegetation cover, patch size
30 distribution, biomass and hydraulic resistance. The main advantages are that the method is: (i)
31 suitable for continuous and discontinuous vegetation covers (ii) of very-high spatial and flexible
32 temporal resolution, (iii) relatively fast compared to conventional ground survey methods, (iv)
33 non-destructive, (v) relatively cheap and easy to use, and (vi) the software is widely available and
34 similar open source alternatives exist. The study area should be less than 10 m wide and the
35 prevailing light conditions and water turbidity levels should be sufficient to look into the water.
36 Further improvements of the images processing are expected in the automatic delineation and
37 classification of the vegetation patches.

38
39 **Key words:** macrophytes, vegetation cover, very high spatial resolution, flexible temporal
40 resolution

41

42 **Introduction**

43 The presence of aquatic vegetation in river ecosystems tends to be highly variable in space and
44 time. Because of the importance of vegetation in fluvial ecosystems there is a need to efficiently
45 map and monitor this variability. The study described in this paper presents a method for detailed
46 mapping of the dynamic vegetation patterns in rivers.

47
48 Macrophytes, or aquatic plants, have different growth forms: exclusively submerged, submerged
49 with floating leaves, exclusively floating or emergent. They occur in single species beds with a
50 continuous cover or in a discontinuous composition of multiple species. The interaction between
51 vegetation and water flow leads to spatial patterns of vegetation patches at reach scale, river
52 sections of 100 to 200 m (Schoelynck et al. 2012). A macrophyte patch can be defined by an area
53 covered by vegetation, which has a finite spatial extent that is larger than an individual shoot but
54 smaller than the entire reach. The size of these vegetation patches varies strongly from a few square
55 decimetre to a few square meter (Gurnell et al. 2006; Sand-Jensen et al. 1999). The size of the
56 individual leaves ranges from several square centimetre to several square decimetre. In temperate
57 mid-latitude climate zones, the development of these vegetation patches has an annual cycle with
58 abundant plant growth in the growth season followed by die-back (Battle and Mihuc 2000;
59 Menendez et al. 2003).

60
61 These dynamic growth processes result in frequent changes in key properties of vegetated rivers
62 including vegetation cover, patch size distribution, biomass and hydraulic resistance. These
63 properties in turn affect stream processes, such as: nutrient cycling (Dhote and Dixit 2009; Krause
64 et al. 2011; Seitzinger et al. 2006), the transport of dissolved matter and the retention of particulate

65 matter (Cordova et al. 2008; Horvath 2004; Lamberti et al. 1989), bedload sediment transport
66 (Gibbins et al. 2007) and drift of macro-invertebrates (Extence et al. 1999).

67

68 The first of the key properties, macrophyte cover, is an essential parameter used for monitoring of
69 fluvial ecosystems. Macrophytes are for example used as a quality parameter in the assessment of
70 the ecological status of surface water for the Water Framework Directive in Europe (EU 2000).
71 This assessment takes into account the number of species and species abundance. The second key
72 property, the frequency distribution of patch sizes, can be used to investigate spatial self-
73 organisation in river ecosystems. Spatial self-organisation in rivers is the process where large scale
74 patterns develop from disordered initial conditions through small scale feedbacks between plants
75 and the water flow (Lejeune et al. 2004; Rietkerk et al. 2004; Schoelynck et al. 2012). The process
76 is important for ecosystem functioning, since self-organised ecosystems have a higher resilience
77 and resistance to environmental change and a higher productivity compared to homogeneous
78 ecosystems (van de Koppel et al. 2008). Schoelynck et al. (2012) showed the presence of spatial
79 self-organisation of macrophytes patches in lowland rivers. They demonstrated that the size
80 distribution of macrophytes patches can be described by a power-law relationship, which is an
81 indication of self-organisation (Newman 2005; Scanlon et al. 2007). Thirdly, biomass is a crucial
82 parameter in many ecological studies for example for the calculation of mass balances or
83 quantification of nutrient fluxes (Borin and Salvato 2012; Dinka et al. 2004). The parameter values
84 will depend on vegetation extent and species composition. Finally, the hydraulic resistance of a
85 river reach is influenced by obstructions like aquatic vegetation, bed material, the meandering of
86 the river and irregularities in its cross-sections (Chow 1959). Macrophytes increase the hydraulic
87 resistance which leads to reduced stream velocities and increased water levels upstream (De
88 Doncker et al. 2009b). A direct effect of increased water levels is a higher risk of flooding. The

89 effect of macrophytes on the hydraulic resistance is threefold: through vegetation density (e.g.
90 biomass (De Doncker et al. 2009b)), plant characteristics (e.g. growth form (Bal et al. 2011)) and
91 spatial distribution (e.g. cross-sectional blockage (Green 2005b)). In general: high biomass, stiff
92 plants and large cross-sectional blockage all lead to a higher resistance to water flow, which is
93 expressed by a higher Manning roughness coefficient (n) (Chow 1959; Madsen et al. 2001;
94 Vereecken et al. 2006). Recently more detailed hydrodynamic models have been developed, which
95 incorporate such plant features (Verschoren et al. 2016).

96
97 To quantify the above-mentioned vegetation parameters and use them for monitoring, modeling
98 and management of river processes, a method is needed that can efficiently map the dynamic
99 patchiness of macrophytes in rivers with a very-high spatial (subcentimetre) and flexible temporal
100 resolution. The detection of fine scale details in structure, texture and pattern on very-high spatial
101 resolution image data allows identification of macrophytes up to species level (Bryson et al. 2013;
102 Visser et al. 2013). Properties like biomass and hydraulic resistance depend strongly on species
103 composition and need flexible temporal resolution (e.g. monthly) data acquisition to catch seasonal
104 variation. Low-altitude image data collection seems the most suitable method to obtain high spatial
105 and flexible temporal resolution data while minimizing the time and cost (Carter et al. 2005;
106 Legleiter 2003).

107
108 High resolution low-altitude image data collection techniques proved to be suitable for many
109 ecological studies in intertidal marine environments with a spatial extent between 0.01 - 1 ha and
110 resolutions ranging between 0.5 - 5 cm. Examples are patterns of algae distribution (Guichard
111 2000), biophysical control of benthic diatom films and macroalgae (van den Wal 2014), the
112 distribution of eelgrass and blue mussel (Barrell and Grant 2015), and terrain models of intertidal

113 rocky shores (Bryson 2013). However, images were mostly obtained at low tides while study sites
114 were not inundated. Due to the absorption of light in water (Visser et al. 2013), limited spatial
115 resolution or high costs (Flynn and Chapra 2014; Husson et al. 2014; Shuchman et al. 2013), it is
116 only relatively recently that more studies started looking at mapping aquatic vegetation in
117 submerged environments, including rivers and lakes (Anker et al. 2014; Silva et al. 2008; Villa et
118 al. 2015). Hyperspectral remote sensing is successfully used to measure the river morphology
119 (Tamminga et al. 2015), to map invasive aquatic vegetation in a delta (Hestir et al. 2008) and
120 submerged macrophytes and green algae in rivers (Anker et al. 2014). However, these
121 hyperspectral images are costly and/or have too low spatial resolution (~1-3 m) to be applied in
122 small streams (stream width <10 m) (Shuchman et al. 2013).

123
124 Recent efforts have been undertaken to obtain low-cost, high spatial resolution (subdecimetre to
125 submetre) images, but with a low spectral range. At a resolution of 25 cm, Flynn and Chapra (2014)
126 mapped aquatic submerged vegetation and green algae in small lowland rivers and lakes, and
127 Nezlin et al. (2007) mapped algae and mussels on tidal flats. Higher spatial resolution images were
128 obtained by Husson et al. (2014) (5.6 cm) and Anker et al. (2014) (4 cm) to record aquatic
129 vegetation. However, these resolutions are often still too coarse to distinguish different macrophyte
130 species, which sometimes requires assessment of the shape of individual leaves. A common
131 recommendation from several of the before mentioned studies is the requirement that images
132 should be taken under optimal conditions, e.g. no diffuse light, sun at its highest position, clear
133 water, no ripples. However, this almost never occurs in reality and therefore further limits the
134 applicability of the method and is an additional reason why this technique has not yet become
135 mainstream in river ecosystem research: it is difficult to look into a river trough a camera lens
136 (Visser et al. 2013).

137
138 In this paper we present a rapid and cost-effective digital aquatic vegetation cover photography
139 technique based on orthogonal low-altitude images with a very-high (subcentimetre) spatial
140 resolution and flexibility to collect data frequently (monthly or higher) under optimal weather and
141 scene illumination conditions (no diffuse light and the sun at its highest position). We use the
142 collected images to map the spatial distribution of aquatic vegetation at species level in two river
143 ecosystems (± 200 m river reaches) and we demonstrate how the maps are suitable to monitor four
144 key properties of vegetated lowland rivers, namely vegetation cover, patch size distribution,
145 biomass and hydraulic resistance.

146 **Materials and methods**

147 **Study area**

148 The data were collected in 2013 in two lowland rivers in the North East of Belgium: Zwarte Nete
149 and Desselse Nete ($51^{\circ} 15' 3.45''$ N, $5^{\circ} 4' 54.27''$ E) (Fig. 1). Both rivers are characterised by
150 extensive plant growth in summer and are surrounded by pasture, which limits overhanging and
151 other riparian vegetation. The rivers have a low suspended matter concentration ($< 50 \text{ mg L}^{-1}$) and
152 the substrate consists of sand (median grain size of $167 \mu\text{m}$). The Zwarte Nete has a mean width
153 of 4.4 m, water depth ranges between 0.5 - 0.6 m and discharge between $0.2 - 0.5 \text{ m}^3 \text{ s}^{-1}$. A reach
154 of 187 m (821 m^2) was mapped where multiple plant species were present. The Desselse Nete is
155 slightly larger with a mean width of 5.4 m, mean water depth of 0.6 - 0.7 m and mean discharge
156 between $0.3 - 0.6 \text{ m}^3 \text{ s}^{-1}$. Here a reach of 180 m (1123 m^2) was selected, dominated by a single
157 submerged species with floating leaves: *Potamogeton natans* (L.). The following species were
158 present in one or both reaches: submerged species: *Callitriche obtusangula* (Le Gall),
159 *Myriophyllum spicatum* (L.), *Potamogeton pectinatus* (L.) *Ranunculus peltatus* (L.), *Sagittaria*

160 *sagittifolia* (L.), *Sparganium emersum* (L.) and emergent species: *Typha latifolia* (L.) and riparian
161 vegetation (not identified to species level). No exclusively floating species were present.

162

163 **Image collection**

164 The images were collected with a Nikon D300s DSLR camera with a crop sensor
165 (Nikon Corporation, 2009). As inherent to most unmodified cameras, images consisting of three
166 broad spectral bands are obtained (RGB): a blue (400 - 500 nm), a green (500 - 600 nm) and a red
167 band (600 - 700 nm). The files were compressed as JPEG (fine) with an image dimension of 4288
168 x 2848 pixels and an image size of 12.3 megapixels. The camera was equipped with a Tokina AT-
169 X 116 Pro DX (11-16mm, F2.8) wide angle lens that has a large field-of-view and a distortion of
170 0.6% (Dxomark). The zoom was set to the widest possible angle and the focus at infinity. The
171 camera was attached with a ball head to a handheld telescopic pole to take low altitude images of
172 the water surface at nadir (Fig. 2a). The lower end of the pole was placed at the river bank. The
173 pole was tilted so that the camera was positioned above the center line of the river at a height of
174 approximately 5 m above the water surface (Fig. 2b). The camera was remotely operated from a
175 laptop (tethered capture), which also provided live view to ensure correct positioning of the image
176 footprint. Both river banks had to be visible in each image. No polarization filter was used as this
177 was not thought to have an effect with the camera at nadir position. Camera ISO was set to 200 to
178 minimize the noise and a variable aperture to achieve a fast shutter speed (Pekin and Macfarlane
179 2009). The images generally covered an area of 10 m (along the stream) x 6.5 m (across) (Fig. 3a
180 and 3b).

181

182 Multiple images were collected at monthly intervals covering the entire reaches of both rivers from
183 April to September 2013. The distance between two consecutive images was 4 m to ensure

184 sufficient overlap (~30 % overlap). Data was collected on clear days around noon to achieve
185 optimal illumination conditions. The angle between the sun and the camera is approximately 40°
186 between 11 a.m. and 1 p.m. (summertime) in Belgium. Several ground controls points (GCPs) were
187 positioned along the reaches to allow georeferencing of the image mosaics. Both reaches are
188 bounded upstream and downstream by small bridges which were included as GCPs. Geographic
189 coordinates for the GCPs were obtained with a dGPS (Trimble R4 GNSS, Eersel, NL) with an
190 accuracy of 1 cm. The exact coordinates of the river banks were once measured with an electronic
191 theodolite (Total Station, Sokkia set 510k, Capelle a/d Ijssel, NL) with a spatial interval of 2 to 3
192 m. The coordinates of the river bank were considered as complementary GCPs, which are clearly
193 visible on the images.

194

195 **Spatio-temporal vegetation cover**

196 Three steps are needed to create vegetation maps at species level: (i) image dehazing and stitching
197 by month and reach, (ii) georeferencing of image mosaics, and (iii) manual delineation of
198 vegetation patches.

199 Firstly, haze was removed from the images with the Autopano Giga (v. 3.0, Kolor, Francin, FR)
200 software using the Neutralhazer Light Anti-Haze plug-in. The software was then used to create
201 image mosaics along the full river reaches, using image matching algorithms to match up
202 overlapping photographs. For around 10 % of the images the matching process seemed to be
203 affected by reflection, movement of the vegetation with the river current and a homogeneous
204 riparian margin. In these cases we manually added extra control points at matching locations in
205 both images. This hardly affected the time to stitch. The image mosaics were exported as a JPEG.
206 This protocol was repeated for the images of both reaches and for each month. Secondly, in ArcGIS
207 (v. 10.1, ESRI Inc, Redlands, USA) the image mosaics were georeferenced using a spline

208 transformation. It should be noted that the GCPs were not present in all images that formed a
209 mosaic. An example of georeferenced image mosaics is given in Fig 3c and 3d. Thirdly, polygons
210 were drawn manually delineating the vegetation patches. Advantages and limitations of this
211 approach are extensively discussed at the end of this paper. Patches consisted of a single species
212 and had a minimum size of 2 dm². For each polygon the type of species was determined from the
213 image (Fig. 3e and 3f). The surface area of each polygon was calculated and summed to obtain the
214 total vegetation cover per reach and per species type.

215
216 The manual image classification was validated against independent field measurements of
217 vegetation presence. A conventional grid method (Anker et al. 2014; Champion and Tanner 2000)
218 was used to estimate macrophyte cover on the ground. A rectangular grid of 2.88 by 0.88 m (36 by
219 11 cells of 0.08 by 0.08 m) was placed at a fixed location monthly in both streams on the same
220 days the images were collected. The presence of macrophytes in each cell is recorded and
221 determined to species level. The image data was resampled to 0.08 m resolution with each cell
222 coded according to the dominant species. The overall accuracy is calculated by comparing the
223 species in each cell of both grids with a true or false evaluation. This is done per month per river.
224 The relative cover for each vegetation class is given for the months with a cover accuracy of less
225 than 95 %.

226
227 **Patch size distribution**

228 We tested if the frequency distribution of patch sizes can be approached by a power-law
229 relationship. We therefore used the inverse cumulative distribution which is the probability that a
230 patch size (S) is larger than or equal to s (Newman 2005; Scanlon et al. 2007):

$$231 \quad P(S \geq s) \sim s^{-\beta} \quad \text{Eq. 1}$$

232 with s the size of a patch and β the power-law exponent. A power-law relationship in this context
233 means that the sizes of patches varies strongly with many small patches and relatively few large
234 patches. R (R Core Team 2014) version 3.2.0, was used to fit a standard least squares regression
235 on the log-transformed data.

236

237 **Biomass**

238 A conversion factor between cover and biomass can be obtained from the literature (e.g. Flynn et
239 al. 2002; Madsen and Adams 1989). However the required input data weren't available for species
240 in our study area, therefore the four dominant species in both rivers (*C. obtusangula*, *M. spicatum*,
241 *P.natans*, *S. emersum*) were sampled monthly to obtain the monthly conversion factor
242 biomass:cover (Tab. 7). Vegetation samples were collected at the date of image acquisition,
243 downstream from the studied reaches to not destruct the natural growth of the vegetation within
244 the study reaches. Each month, three replicates per species were sampled by manually removing
245 the above ground vegetation in a quadrant of 0.5 m x 0.5 m that was placed upon a monotopic
246 vegetation patch. The samples were oven dried (at 70° C for 48 h) and weighed afterwards (dry
247 weight, DW). It has to be noted that in May 2013, no sample could be taken for *C. obtusangula*.
248 Therefore the average was taken of values for April and June to estimate the biomass in that month.
249 The total cover per species per month was obtained through the image analysis. Then the biomass
250 (gDW) per species was calculated monthly by multiplying the species-specific conversion factor
251 biomass:cover (gDW m⁻²) with the corresponding cover (m²) . The biomass values were summed
252 for the whole reach and divided by the total surface of the reach to obtain the total biomass (gDW
253 m⁻²) averaged out over all species and over the whole river reach. Since three replicates were taken,
254 the total biomass consists of three values.

255

256 The applied image analysis method aims to quantify vegetation cover in a non-destructive way.
257 However, the validation of the total biomass required mowing of all the vegetation and is therefore
258 a destructive method. We only had the opportunity to use the mowing method in August. On 26
259 and 28 August 2013 the entire reach in the Desselse Nete and Zwarte Nete was mechanically
260 mowed by cutting most vegetation just above the sediment and removing it from the river. All
261 mowed vegetation from both reaches was immediately weighed (fresh weight, FW). A
262 representative subsample of the biomass consisting of a mixture of all species, was transported to
263 the lab. The subsample was weighed (FW), dried at 70°C for 48h and reweighed (DW). This
264 enabled us to determine a conversion factor between FW and DW for the biomass of the entire
265 reach. R 3.2.0 was used to perform a one-sample t-test to test the difference between the total
266 biomass obtained by the mowing method (one value) and by the image method (mean with standard
267 error based on three values).

268

269 **Hydraulic resistance**

270 The hydraulic resistance of rivers can be expressed as a Manning coefficient (Chow 1959). The
271 commonly used equation to calculate the Manning coefficient is based on hydraulic parameters and
272 is applicable in vegetated and non-vegetated rivers (Eq. 2, Tab. 1) (Chow 1959). The equation uses
273 the cross-sectional area, discharge, hydraulic radius and the water level slope. The water discharge
274 was measured upstream of both reaches at the same days the images were taken, using an
275 electromagnetic flow meter (Valeport model 801, Totnes, UK) and calculated by the velocity-area
276 method (Bal and Meire 2009). Simultaneously, the water level was measured with two pressure
277 sensors (Eickelkamp, Geisbeek, NL) placed in the water column near the bridges bordering the reach
278 upstream and downstream with a time interval of 20 min. and with an accuracy of 0.5 cm. The
279 elevation difference between the pressure sensors was measured with a RTK-GSP. The water levels

280 are corrected for atmospheric pressure and averaged over 24 h for each sampling campaign. The
281 water level slope in the reaches was calculated by subtracting the upstream and downstream water
282 level, divided by the length of the reach. Additionally, different empirical relationships are used to
283 convert vegetation properties to the Manning coefficient. Based on the data of the surface area
284 coverage of Green (2005a) we found an empirical relationship (Eq. 3, Tab. 1) between the Manning
285 coefficient and the vegetation cover. De Doncker et al. (2009a) fitted an equation (Eq. 4, Tab. 1)
286 based on measurements of the biomass (gDW m^{-2}) and the Manning coefficient. These empirical
287 relationships (Eq. 3 and Eq. 4) are easy to use, but have a limited application potential. They don't
288 account for the species composition and the horizontal and vertical distribution of the vegetation and
289 are derived for a specific study area. The general Manning coefficient (Eq. 2) is used to validate the
290 empirical equations (Eq. 3 and Eq. 4).

291 **Results**

292 Between 86 and 115 images (~ 1.9 pixels cm^{-2} , ~ 1.3 cm edge length) were taken per reach from
293 which 41 to 56 were selected to construct the image mosaic. The images collection took around
294 one hour per reach per sampling campaign. Reduced illumination of the submerged vegetation
295 target for the April and September data due to low sun angles, made macrophytes less visible in
296 the images. Delineation of the vegetation patches was still possible but the vegetation cover may
297 have been underestimated. Processing of the images took around two days for months with a low
298 vegetation abundance ($< 30\%$) and around three days for months with a high vegetation cover ($>$
299 30%).

300

301 **Spatio-temporal vegetation cover**

302 The total vegetation cover and partial species cover is given per month for the two reaches (Fig.
303 4). In the Zwarte Nete, the total vegetation cover increases from April to August and suddenly
304 decreases in September due to the scheduled mowing event on 28 August 2013. The dominant
305 species in the Zware Nete are *S. emersum* and *M. spicatum* during the sampling period (Fig. 4a).
306 The natural development of the vegetation cover in the Desselse Nete is different. The growth was
307 disturbed by an extra mowing activity on 25 June 2013 for management and safety regulations.
308 Two months later, a scheduled mowing event took place on 26 August 2013. *P. natans* is the most
309 abundant species in the Desselse Nete each month and recovered completely 8 weeks after the first
310 mowing event (Fig. 4b).

311 The validation of the image method with the ground survey showed that the accuracy of species
312 identification is very high (>97 %) in the study reach dominated by a single species (Desselse Nete)
313 (Tab. 2). These high values are due the relative simple composition of the vegetation patches, where
314 the whole reach is covered by a single species. On the contrary, the accuracy is less (> 59%) in the
315 river with a heterogeneous composition of multiple species, certainly in months when the
316 vegetation patches are developing (June and July). So the accuracy to determine the exact location
317 of vegetation patches is limited in those months.

318 For those months with a cover accuracy less than 95 %, the relative cover of each vegetation class
319 is given separately in Tab. 3. The difference in cover between the ground survey method and the
320 image method for each vegetation class is less than 12 %. This means that the cover per vegetation
321 class agrees well between both methods.

322

323 **Patch size distribution**

324 In total 262 vegetation patches were mapped in August in the Zwarte Nete, of which 143 were *C.*
325 *obtusangula* patches. The surface area of these patches ranged between 0.04 m² and 2.76 m². The
326 size frequency distribution of the patches is plotted on a double logarithmic scale (Fig. 5). A
327 significant power-law relationship was found for the upper part of the distribution (least squares
328 regression on the log-transformed data; $p < 0.001$, $R^2 = 0.99$; 59 % of the data).

329

330 **Biomass**

331 The total biomass per reach is estimated with the image analysis method on a monthly basis (Tab.
332 4). The monthly conversion factors are given in Tab. 7. The mowed vegetation is immediately
333 weighed (FW) and converted to dry weight with measured the conversion factor FW:DW equal to
334 10.3. The total biomass (gDW m⁻²) obtained by the image analysis method does not significantly
335 differ from the biomass (gDW m⁻²) obtained by the mowing method. The results of the one-sample
336 t-test is a p-value of 0.797 and 0.198 for the Zwarte Nete and Desselse Nete, respectively.

337

338 **Hydraulic resistance of vegetated rivers**

339 Variation of the Manning coefficient over time is shown for the Zwarte Nete and Desselse Nete in
340 Figure. 6. In the Zwarte Nete the Manning coefficient is based on hydraulic data, Eq. 2, increasing
341 from April to August and decreasing in September to values similar to those of April. The Manning
342 coefficients of the Zwarte Nete calculated with the empirical equations (Eq. 3 and Eq. 4) are well
343 in agreement. The largest difference is found in August with values of 0.26, 0.30 and 0.20 for Eq.
344 2, Eq. 3 and Eq. 4, respectively. The Manning coefficient based on hydraulic data, Eq. 2, varies
345 between 0.03 and 0.17 in the Desselse Nete. The empirically based Manning coefficients

346 overestimate this value every month up to a factor two. The largest differences are found in the
347 months May, June and August.

348 **Discussion**

349 There is a strong need for new methods to acquire 2D data on the spatial and temporal distribution
350 of vegetation in small rivers. The digital cover photography technique applied in this paper is a
351 useful tool to obtain this detailed 2D information. This method has six main advantages: (i) it can
352 be applied in rivers with any kind of vegetation cover; (ii) it has a very-high spatial resolution,
353 around 1.9 pixels cm^{-2} (~1.3 cm edge length), and a very flexible temporal resolution with the
354 frequency only dependent on availability of suitable weather conditions; (iii) it is relatively fast,
355 two to three days to collect and process the data of a reach of 180 m; (iv) it is non-destructive in
356 contrast to other methods where sampling is involved; (v) the equipment is relatively cheap with a
357 single time cost of approximately € 2000 for the camera, lens, control software and memory card;
358 (vi) the software used to process the data is widely available and similar open source alternatives
359 exist. Tab. 5 shows the performance of the current method in comparison to five other commonly
360 used remote sensing approaches with optical imagery. The spectral range and spectral resolution
361 depends on the sensor for all platforms mentioned in Tab. 5. Manned aircraft imaging can have a
362 wide range of spectral resolution from very narrow band hyperspectral imagery to one very broad
363 band for a panchromatic image. Similarly for satellite imagery, sensors with a high spectral
364 resolution are available. However, these images are of low spectral quality and low spatial
365 resolution. Hyperspectral sensors with a high spectral resolution are available for unmanned aerial
366 vehicles but can only be assembled on larger vehicles and do not achieve the high spatial resolution
367 that can be obtained with RGB cameras. The current method is particularly suitable for studies in
368 river reaches which are difficult to access and require high spatial resolution . In addition, limited

369 technical training is required to pre- and post-process the images. The method can be used in its
370 current stage in relative small study areas for monitoring, modelling and management purposes.
371 Applying this method in larger study areas would require further automatization of image
372 collection, e.g. by attaching the camera to an Unmanned Aerial Vehicle (UAV) (Husson et al. 2014;
373 Tamminga et al. 2015), and image classification, e.g. by applying the OBIA method (Visser et al.
374 2016).

375 The image data collection requires suitable light and site conditions. The water needs to be clear
376 (i.e. ideally < 1 m deep and low turbidity) (Visser et al. 2013), and the water velocity should be
377 low to limit stem motion (i.e. ideally < 1 ms⁻¹) (Franklin et al. 2008). These site conditions are
378 similar requirements for the occurrence of macrophytes in the first place (Riis and Biggs 2003).
379 However the water can be temporary less clear after storm events. In this case it is recommended
380 to wait a few days until the concentration of suspended sediment is reduced. Light intensity should
381 be sufficient to penetrate the surface and illuminate the submerged macrophytes. The angle
382 between the sun and the camera should be around 45° to minimize sun glint and maximize the light
383 availability in the water. The time of image collection depends on the latitude of the study area, for
384 example in Belgium (latitude 52 °) this is around noon, between 11 a.m. and 1 p.m., summertime.
385 The image collection can only take place under these specified good weather conditions. This limits
386 the data collection frequency, but for monitoring vegetation very high frequency data is rarely
387 needed. Techniques currently under development may in the near future allow the removal of
388 remaining surface reflection (Hardesty 2015). Other requirements are related to the study area
389 itself. The rivers and streams should be relative small, i.e. < 10 m wide, which is the equivalent of
390 the spatial extent covered by one image, and at least one river bank should be accessible and stable
391 enough to position the pole. Yet these limitations to the study area can be overcome by attaching
392 the camera to an Unmanned Aerial Vehicle (UAV) (Husson et al. 2014; Tamminga et al. 2015), or

393 to a helium balloon, or by attaching the pole to the bow of a boat (Lirman and Deangelo 2007).
394 This makes it possible to collect similar resolution data from close to the water surface of larger
395 rivers. However, helium balloons need to be sufficiently big to carry a DSLR camera, which makes
396 them rather impractical and in the long-run quite expensive platforms (due to the cost of helium).
397 UAVs are a good alternative since battery life is improving year on year. Currently the only
398 disadvantages of a rotary-winged UAV platform are (i) the need for training to actually fly the
399 vehicle, which may involve some costly training; (ii) the purchase and insurance of suitable quality
400 UAV and camera; (iii) the transport of larger UAVs. UAVs are therefore the platform of choice
401 for further development of the method proposed in this paper.

402
403 The image processing as it was done in this study works well, yet improvements are possible to
404 delineate and identify the vegetation patches. This study used a manual interpretation based on
405 expert judgement, which is a sound method to separate between different species (Husson et
406 al.2014), because the manual delineation and identification uses many image elements like size,
407 shape, shadow, colour, texture, pattern, location and surroundings (Colwell 1960; Tempfli et al.
408 2009). However, the observer bias can still be present since this method makes use of manual
409 decision rules concerning the exact edge of the vegetation patches. In the study reach dominated
410 by a single species the accuracy is very high (>97 %). These high values are due to the relative
411 simple composition of the vegetation patches, where the whole reach is covered by a single species
412 (Desselse Nete). On the contrary, the accuracy is less (> 59%) in the river with a heterogeneous
413 composition of multiple species (Zwarte Nete), certainly in months when the vegetation patches
414 are developing (June and July). If we compare the relative cover of each vegetation class between
415 the image method and ground survey, differences are less than 12 %. The images method proved
416 to be suitable to estimate the relative cover of each vegetation class in rivers with a continuous and

417 discontinuous vegetation cover. However, it is difficult to map the exact location of all vegetation
418 patches in rivers with heterogeneous vegetation cover. This is due to the movement of the
419 vegetation patches by the flowing water and the relatively simple image processing.

420
421 Another limitation is the detection of rare species which are normally not abundantl, e.g. *C.*
422 *obtusangula* was detected by the ground survey in June and July in the Zwarte Nete but not by the
423 image method. The last limitation is the separation of multi-layered plant communities, e.g. *P.*
424 *natans* was classified as *S. emersum* in August (Desselse Nete), while only a few leaves of *S.*
425 *emersum* where present on top of *P. natans*. Similar limitations are found by Anker et al. (2014).
426 From the images, plant growth form (submerged, submerged with floating leaves, emergent) can
427 be easily recognized, as well as the species identification up to genus level. A classification up to
428 species level is possible, but requires knowledge of the species present in the reach. This
429 information can simply be obtained during the collection of the images at the field site. Automatic
430 classification methods based on variation in spectral signatures of different vegetation types could
431 not be used to automatically delineate and identify vegetation patches under these specific
432 circumstances. The varying incidences of light, the prevailing sub-optimal light conditions during
433 the sampling campaign and submergence depth of the vegetation all caused complications for
434 automated species detection (Visser et al. 2013). We acknowledge this drawback on the manual
435 image processing, which increases the cost of data processing and may make this method no longer
436 as cost-effective. Attention should be given to reduce phenological (space and time) differences in
437 the classification to make this technique suitable for long term monitoring. Two solutions have
438 been proposed: (i) convert the Red-Green-Blue colors to the green chromatic coordinate
439 ($G/[R + G + B]$), (ii) use the 90th percentile of all daytime values within a three-day window around
440 the centre day (Dronova 2017; Sonnentag et al. 2012). However, it may be not straightforward to

441 apply similar algorithms to submerged aquatic vegetation where relative variation in Red-Green-
442 Blue values at any point can differ due to water depth differences. Alternative image analysis
443 approaches such as object based image analysis (OBIA) are less reliant on spectral information and
444 may mitigate for such conditions, however applications of such approaches in submerged
445 environments are still in a developmental stage (Visser et al. 2016). OBIA is currently applied in
446 other ecosystems. For example Laba et al. (2010) used a maximum-likelihood classification in tidal
447 marshes, which resulted in a classification accuracy between 45 and 77 %. In offshore submerged
448 environments OBIA based approaches have so far achieved good results for mapping coarse
449 vegetation and substrate classes. For example, the extent of seagrass habitat was mapped by
450 Baumstark et al. (2016), showing in a slightly higher accuracy using OBIA (78%) compared to
451 photo-interpretation (71%).

452 The image analysis method proved suitable for measuring the spatio-temporal vegetation cover,
453 which is a primary parameter for monitoring vegetated ecosystems. For instance within the Water
454 Framework Directive, it is essential for long-term monitoring of vegetation abundance (Hering et
455 al. 2010). Changes in abundance and location of the vegetation were derived directly from the
456 image data. For example the regrowth capacity of *P. natans* was high after the mowing event in
457 June, and pre-mowed cover values were reached within 8 weeks, which is similar to other
458 macrophyte species (Bal et al. 2006). Other, more conventional methods to estimate vegetation
459 cover data range from fast methods with a high observer bias due to expert judgement (Tansley
460 scaling method based on 5 classes) to more detailed scaling methods, which have a higher accuracy,
461 but are more time consuming and require substantial expert knowledge (Braun-Blanquet scaling
462 method based on 9 classes (Blanquet 1928)) and Londo scaling method based on at least 21 classes
463 (Londo 1976)). These methods have two main disadvantages. Firstly, abundance class errors are
464 difficult to correct even with substantial expert knowledge (Wiederkehr et al. 2015). Secondly, the

465 classification of the cover makes use of discontinuous class scales, which are less accurate and can
466 hamper data analyses. Hence the image analysis method fulfils the requirement of a more objective
467 quantification of the cover with a continuous cover scale with high spatial and flexible temporal
468 resolution.

469
470 The cover maps were also used in this study to investigate the presence of spatial self-organisation
471 of macrophytes in lowland rivers. A significant power-law relationship of the frequency
472 distribution of the patch sizes is found, which is an indication of spatial self-organisation (Newman
473 2005; Scanlon et al. 2007). This is in agreement with a study of Schoelynck et al. (2012), who
474 investigated the spatial self-organisation of macrophytes in the same reach in the Zwarte Nete in
475 2008. In the study of Schoelynck et al. (2012) the exact location of all vegetation patches was
476 determined using an electronic theodolite. It took roughly three weeks to map the whole reach,
477 which is much slower in comparison with the new method, where we needed 1 hour to collect the
478 images and two to three days to process the data. So obtaining spatial information of vegetation is
479 much faster compared to conventional methods.

480
481 From the cover data, biomass can be derived using simple non-destructive cover:biomass
482 conversion factors. These conversion factors can be determined for the specific field site or can be
483 obtained from literature (e.g. Madsen and Adams (1989); Flynn et al. (2002)). The biomass (gDW
484 m⁻²) estimated by the image analysis method was compared to the biomass obtained from the
485 scheduled mowing method. The biomass obtained by the two methods does not significantly differ
486 for either of the two reaches. The relatively small differences may be attributed to inaccuracies in
487 both methods. During the scheduled mowing, the biomass could have been slightly overestimated
488 when non-plant materials like sediment, stones and dead wood were removed too, which may have

489 added up to the total fresh weight, or underestimated the latter when not all the vegetation was
490 removed. However, we only assessed the biomass in a month with high biomass. Higher relative
491 difference in biomass might be expected when less biomass is present, but this would result in low
492 absolute differences. The image analysis method may also have certain flaws and uncertainties
493 involving the estimation of the species-specific biomass obtained by the plots. The within species
494 variation of the biomass may not be fully captured by three replicas (e.g. by depth variance of the
495 river and of the vegetation). The image analysis method doesn't account for variability in the
496 density. Classic methods of biomass estimation are based on destructive measures of the biomass
497 (mowing, harvesting), which disturb the follow-up of natural vegetation development during the
498 growth season (Wood et al. 2012).

499
500 The difference between the Manning coefficient based on empirical relationships and the one based
501 on hydraulic data differs less than 23 % in the Zwarte Nete and less than 37% in the Desselse Nete.
502 The empirical relationships don't account for the species composition and horizontal and vertical
503 distribution of the vegetation, which are different in both rivers and are major determining factors
504 of the hydraulic resistance of the reach. The Zwarte Nete is dominated by submerged vegetation
505 and this vegetation type has similar effects on the hydraulic resistance as the vegetation used to
506 construct Eq. 2 and Eq. 3. The Desselse Nete is dominated by the floating species *P. natans*, which
507 is a more open species that concentrates the majority of the biomass near the water surface, which
508 leads to a limited interaction with the water flow: rivers with macrophytes can have a 2 to 7-fold
509 increase of the resistance for floating (Green 2005a) and submerged (Bal and Meire 2009) species,
510 respectively, compared to rivers without vegetation. The same vegetation biomass or cover will
511 therefore result in a lower hydraulic resistance. Detailed 2D hydrodynamic models can be used to
512 quantify more accurately the hydraulic resistance created by the vegetation based on plant density,

513 species characteristics and spatial distribution of the vegetation (Verschoren et al. 2015). Accurate
514 2D spatio-temporal vegetation cover data, as obtained by the digital cover photography technique,
515 is indispensable to calibrate and validate these models. The spatial distribution of the vegetation is
516 a direct input to these models. Therefore these models account for the exact location of all
517 vegetation patches and the different plant characteristics of all species. This is a major leap forward
518 for engineers and water managers in the fine tuning of the hydrodynamic models of vegetated
519 rivers.

520 **Conclusions**

521 We successfully applied a digital cover photography technique based on orthogonal aerial images
522 with a very-high spatial (subcentimetre) and flexible temporal (monthly) resolution. The produced
523 vegetation maps were used to assess four key properties of vegetated lowland rivers which are
524 important for monitoring, modelling and management, being spatio-temporal variation in
525 vegetation cover, patch size distribution, biomass and hydraulic resistance.

526 The main limitations are related to the study area itself, which should be limited in size, and the
527 prevailing light conditions should be sufficient to look into the water. Improvements in the images
528 processing are situated in the automatic delineation and classification of the vegetation patches.

529

530 **Acknowledgements**

531 The funding for this research was partly provided by the Research Fund Flanders (FWO-, project
 532 no. G.0290.10) via the multidisciplinary research project ‘Linking optical imaging techniques and
 533 2D-modelling for studying spatial heterogeneity in vegetated streams and rivers’ (University of
 534 Antwerp and University of Ghent) and partly by Province of Antwerp, departement Leefmilieu,
 535 dienst Integraal Waterbeleid (Report number ECOBE – 014 – R179). V.V. thanks the Institute for
 536 the Promotion of Innovation through Science and Technology in Flanders (IWT-Vlaanderen) for
 537 personal research funding. J.S. is a postdoctoral fellow of FWO (project no. 12H8616N).

538

539 **References**

- 540 Anker, Y., Y. Hershkovitz, E. Ben Dor & A. Gasith, 2014. Application of Aerial Digital Photography
 541 for Macrophyte Cover and Composition Survey in Small Rural Streams. *River Res Appl*
 542 30(7):925-937.
- 543 Apollo Mapping, 2016. RapidEye. In. [https://apollomapping.com/imagery/medium-resolution-](https://apollomapping.com/imagery/medium-resolution-satellite-imagery)
 544 [satellite-imagery](https://apollomapping.com/imagery/medium-resolution-satellite-imagery).
- 545 Bal, K. D. & P. Meire, 2009. The Influence of Macrophyte Cutting on the Hydraulic Resistance of
 546 Lowland Rivers. *J Aquat Plant Manage* 47:65-68.
- 547 Bal, K. D., E. Struyf, H. Vereecken, P. Viaene, L. De Doncker, E. de Deckere, F. Mostaert & P.
 548 Meire, 2011. How do macrophyte distribution patterns affect hydraulic resistances? *Ecol*
 549 *Eng* 37(3):529-533.
- 550 Bal, K. D., S. Van Belleghem, E. De Deckere & P. Meire, 2006. The re-growth capacity of sago
 551 pondweed following mechanical cutting. *J Aquat Plant Manage* 44:139-141.
- 552 Barrell, J. & J. Grant, 2015. High-resolution, low-altitude aerial photography in physical geography:
 553 A case study characterizing eelgrass (*Zostera marina* L.) and blue mussel (*Mytilus edulis*
 554 L.) landscape mosaic structure. *Prog Phys Geog* 39(4):440-459.
- 555 Battle, J. M. & T. B. Mihuc, 2000. Decomposition dynamics of aquatic macrophytes in the lower
 556 Atchafalaya, a large floodplain river. *Hydrobiologia* 418:123-136. Blanquet, B., 1928.
 557 *Pflanzensoziologie. Grundzüge der Vegetationskunde*, Berlin 1.ed. Berlin.
- 558 Baumstark R., R. Duffey & R. Pu, 2016. Mapping seagrass and colonized hard bottom in Springs
 559 Coast, Florida using WorldView-2 satellite imagery. *Estuarine, Coastal and Shelf Science*
 560 181:83-92. Borin, M. & M. Salvato, 2012. Effects of five macrophytes on nitrogen
 561 remediation and mass balance in wetland mesocosms. *Ecol Eng* 46:34-42.
- 562 Bryson, M., M. Johnson-Roberson, R. J. Murphy & D. Bongiorno, 2013. Kite Aerial Photography
 563 for Low-Cost, Ultra-high Spatial Resolution Multi-Spectral Mapping of Intertidal
 564 Landscapes. *Plos One* 8(9).
- 565 Carter, G. A., A. K. Knapp, J. E. Anderson, G. A. Hoch & M. D. Smith, 2005. Indicators of plant
 566 species richness in AVIRIS spectra of a mesic grassland. *Remote Sens Environ* 98(2-
 567 3):304-316.

- 568 Champion, P. D. & C. C. Tanner, 2000. Seasonality of macrophytes and interaction with flow in a
569 New Zealand lowland stream. *Hydrobiologia* 441(1-3):1-12.
- 570 Chow, V. T., 1959. Open-channel hydraulics. McGraw-Hill, New York, USA.
- 571 Colwell, R., 1960. Manual of photographic interpretation Washington, DC.
- 572 Cordova, J. M., E. J. Rosi-Marshall, J. L. Tank & G. A. Lamberti, 2008. Coarse particulate organic
573 matter transport in low-gradient streams of the Upper Peninsula of Michigan. *J N Am*
574 *Benthol Soc* 27(3):760-771.
- 575 De Doncker, L., P. Troch, R. Verhoeven, K. Bal, N. Desmet & P. Meire, 2009a. Relation between
576 Resistance Characteristics Due to Aquatic Weed Growth and the Hydraulic Capacity of the
577 River Aa. *River Res Appl* 25(10):1287-1303.
- 578 De Doncker, L., P. Troch, R. Verhoeven, K. Bal, P. Meire & J. Quintelier, 2009b. Determination of
579 the Manning roughness coefficient influenced by vegetation in the river Aa and Biebrza
580 river. *Environ Fluid Mech* 9(5):549-567.
- 581 Dhote, S. & S. Dixit, 2009. Water quality improvement through macrophytes-a review. *Environ*
582 *Monit Assess* 152(1-4):149-153.
- 583 Dinka, M., E. Agoston-Szabo & I. Toth, 2004. Changes in nutrient and fibre content of
584 decomposing *Phragmites australis* litter. *Int Rev Hydrobiol* 89(5-6):519-535.
- 585 Dronova, I. 2017. Environmental heterogeneity as a bridge between ecosystem service and visual
586 quality objectives in management, planning and design. *Landscape and Urban Planning*
587 163:90-106.
- 588 EU, 2000. 2000/60/EC. A framework for the Community action in the field of water policy, or
589 short: The EU Water Framework Directive Directive 2000/60/EC, The European Parliament
590 and the European Council of Ministers. Brussels, Belgium.
- 591 Extence, C. A., D. M. Balbi & R. P. Chadd, 1999. River flow indexing using British benthic
592 macroinvertebrates: A framework for setting hydroecological objectives. *Regul River*
593 15(6):543-574.
- 594 Flynn, K. F. & S. C. Chapra, 2014. Remote Sensing of Submerged Aquatic Vegetation in a Shallow
595 Non-Turbid River Using an Unmanned Aerial Vehicle. *Remote Sens-Basel* 6(12):12815-
596 12836.
- 597 Flynn, N. J., D. L. Snook, A. J. Wade & H. P. Jarvie, 2002. Macrophyte and periphyton dynamics
598 in a UK Cretaceous chalk stream: the River Kennet, a tributary of the Thames. *Sci Total*
599 *Environ* 282:143-157.
- 600 Foody, G. M., 2002. Status of land cover classification accuracy assessment. *Remote Sens Environ*
601 80(1):185-201.
- 602 Franklin, P., M., Dunbar & P. Whitehead, 2008. Flow controls on lowland river macrophytes: A
603 review. *Sci Total Environ* 400(1-3):369-378.
- 604 Gibbins, C., D. Vericat & R. J. Batalla, 2007. When is stream invertebrate drift catastrophic? The
605 role of hydraulics and sediment transport in initiating drift during flood events. *Freshwater*
606 *Biol* 52(12):2369-2384.
- 607 Green, J. C., 2005a. Comparison of blockage factors in modelling the resistance of channels
608 containing submerged macrophytes. *River Res Appl* 21(6):671-686.
- 609 Green, J. C., 2005b. Modelling flow resistance in vegetated streams: review and development of
610 new theory. *Hydrol Process* 19(6):1245-1259.
- 611 Guichard, F., E. Bourget & J. P. Agnard, 2000. High-resolution remote sensing of intertidal
612 ecosystems: A low-cost technique to link scale-dependent patterns and processes. *Limnol*
613 *Oceanogr* 45(2):328-338.

- 614 Gurnell, A. M., M. P. van Oosterhout, B. de Vlieger & J. M. Goodson, 2006. Reach-scale interactions
615 between aquatic plants and physical habitat: River Frome, Dorset. *River Res Appl*
616 22(6):667-680.
- 617 Hardesty, L., 2015. Removing reflections from photos taken through windows: new algorithm
618 exploits multiple reflections in individual images to distinguish reflection from transmission.
619 In: Massachusetts Institute of Technology.
- 620 Hering, D., A. Borja, J. Carstensen, L. Carvalho, M. Elliott, C. K. Feld, A. S. Heiskanen, R. K.
621 Johnson, J. Moe, D. Pont, A. L. Solheim & W. Van De Bund, 2010. The European Water
622 Framework Directive at the age of 10: A critical review of the achievements with
623 recommendations for the future. *Sci Total Environ* 408(19):4007-4019.
- 624 Hestir, E. L., S. Khanna, M. E. Andrew, M. J. Santos, J. H. Viers, J. A. Greenberg, S. S. Rajapakse
625 & S. L. Ustin, 2008. Identification of invasive vegetation using hyperspectral remote
626 sensing in the California Delta ecosystem. *Remote Sens Environ* 112(11):4034-4047.
- 627 Horvath, T. G., 2004. Retention of particulate matter by macrophytes in a first-order stream.
628 *Aquat Bot* 78(1):27-36.
- 629 Husson, E., O. Hagner & F. Ecke, 2014. Unmanned aircraft systems help to map aquatic
630 vegetation. *Appl Veg Sci* 17(3):567-577.
- 631 Krause, S., D. M. Hannah, J. H. Fleckenstein, C. M. Heppell, D. Kaeser, R. Pickup, G. Pinay, A. L.
632 Robertson & P. J. Wood, 2011. Inter-disciplinary perspectives on processes in the
633 hyporheic zone. *Ecohydrology* 4(4):481-499.
- 634 Lamberti, G. A., S. V. Gregory, L. R. Ashkenas, R. C. Wildman & A. D. Steinman, 1989. Influence
635 of Channel Geomorphology on Retention of Dissolved and Particulate Matter in a Cascade
636 Mountain Stream. *Us for Serv T R Psw* 110:33-39.
- 637 Laba, M., B. Blair, R. Downs, B. Monger, W. Philpot, S. Smith, P. Sullivan & P. C. Baveye, 2010.
638 Use of textural measurements to map invasive wetland plants in the Hudson River National
639 Estuarine Research Reserve with IKONOS satellite imagery. *Remote Sensing of*
640 *Environment* 114:876-886.
- 641 Legleiter, C. J., 2003. Spectrally driven classification of high spatial resolution, hyperspectral
642 imagery: A tool for mapping in-stream habitat. *Environ Manage* 32(3):399-411.
- 643 Lejeune, O., M. Tlidi & R. Lefever, 2004. Vegetation spots and stripes: Dissipative structures in
644 arid landscapes. *Int J Quantum Chem* 98(2):261-271.
- 645 Lirman, D. & G. Deangelo, 2007. Geospatial video monitoring of benthic habitats using the
646 Shallow-Water Positioning System (SWaPS). *Oceans-Ieee*:1176-1180.
- 647 Londo, G., 1976. The decimal scale for relevés of permanent quadrats, vol 33.
- 648 Madsen, J. D. & M. S. Adams, 1989. The Distribution of Submerged Aquatic Macrophyte Biomass
649 in a Eutrophic Stream, Badfish Creek - the Effect of Environment. *Hydrobiologia*
650 171(2):111-119.
- 651 Madsen, J. D., P. A. Chambers, W. F. James, E. W. Koch & D. F. Westlake, 2001. The interaction
652 between water movement, sediment dynamics and submersed macrophytes.
653 *Hydrobiologia* 444(1-3):71-84.
- 654 Masek, J. G., D. J. Hayes, M. J. Hughes, S. P. Healey & D. P. Turner, 2015. The role of remote
655 sensing in process-scaling studies of managed forest ecosystems. *Forest Ecol Manag*
656 355:109-123.
- 657 Menendez, M., O. Hernandez & F. A. Comin, 2003. Seasonal comparisons of leaf processing rates
658 in two Mediterranean rivers with different nutrient availability. *Hydrobiologia* 495(1-3):159-
659 169.

- 660 Mitchell, J. J., R. Shrestha, L. P. Spaete & N. F. Glenn, 2015. Combining airborne hyperspectral
661 and LiDAR data across local sites for upscaling shrubland structural information: Lessons
662 for HypsIRI. *Remote Sens Environ* 167:98-110.
- 663 NASA, 2016. MODIS, Moderate Resolution Imaging Spectroradiometer. In.
664 <http://modis.gsfc.nasa.gov>.
- 665 Newman, M. E. J., 2005. Power laws, Pareto distributions and Zipf's law. *Contemporary Physics*
666 46(5):323-351.
- 667 Nezlin, N. P., K. Kamer & E. D. Stein, 2007. Application of color infrared aerial photography to
668 assess macroalgal distribution in an eutrophic estuary, upper Newport Bay, California.
669 *Estuar Coast* 30(5):855-868.
- 670 Pekin, B. & C. Macfarlane, 2009. Measurement of Crown Cover and Leaf Area Index Using Digital
671 Cover Photography and Its Application to Remote Sensing. *Remote Sens-Basel* 1(4):1298-
672 1320.
- 673 R Core Team, 2014. R: A language and environment for statistical computing.
- 674 Rango, A., A. Laliberte, K. Havstad, C. Winters, C. Steele & D. Browning, 2010. Rangeland
675 Resource Assessment, Monitoring, and Management Using Unmanned Aerial Vehicle-
676 Based Remote Sensing. *Int Geosci Remote Se*:608-611.
- 677 Rietkerk, M., S. C. Dekker, P. C. de Ruiter & J. van de Koppel, 2004. Self-organized patchiness
678 and catastrophic shifts in ecosystems. *Science* 305(5692):1926-1929.
- 679 Riis, T. & B. J. F. Biggs, 2003. Hydrologic and hydraulic control of macrophyte establishment and
680 performance in streams. *Limnol Oceanogr* 48(4):1488-1497.
- 681 Sand-Jensen, K., K. Andersen & T. Andersen, 1999. Dynamic properties of recruitment, expansion
682 and mortality of macrophyte patches in streams. *Int Rev Hydrobiol* 84(5):497-508.
- 683 Satellite Imaging Corporation, 2016. Ikonos Satellite Sensor. In.
684 <http://www.satimagingcorp.com/satellite-sensors/ikonos/>.
- 685 Scanlon, T. M., K. K. Caylor, S. A. Levin & I. Rodriguez-Iturbe, 2007. Positive feedbacks promote
686 power-law clustering of Kalahari vegetation. *Nature* 449(7159):209-U4.
- 687 Schoelynck, J., T. De Groote, K. Bal, W. Vandenbruwaene, P. Meire & S. Temmerman, 2012. Self-
688 organised patchiness and scale-dependent bio-geomorphic feedbacks in aquatic river
689 vegetation. *Ecography* 35(8):760-768.
- 690 Seitzinger, S., J. A. Harrison, J. K. Bohlke, A. F. Bouwman, R. Lowrance, B. Peterson, C. Tobias &
691 G. Van Drecht, 2006. Denitrification across landscapes and waterscapes: A synthesis. *Ecol*
692 *Appl* 16(6):2064-2090.
- 693 Shuchman, R. A., M. J. Sayers & C. N. Brooks, 2013. Mapping and monitoring the extent of
694 submerged aquatic vegetation in the Laurentian Great Lakes with multi-scale satellite
695 remote sensing. *J Great Lakes Res* 39:78-89.
- 696 Silva, T. S. F., M. P. F. Costa, J. M. Melack & E. M. L. M. Novo, 2008. Remote sensing of aquatic
697 vegetation: theory and applications. *Environ Monit Assess* 140(1-3):131-145.
- 698 Sonnentag, O., Hufkens, K., Teshera-Sterne, C., Young, A.M., Friedl, M.A., Braswell, B.H., Miliman,
699 T., O'Keefe, J., Richardson, A.D. (2012), Digital repeat photography for phenological
700 research in forest ecosystems. *Agricultural and Forest Meteorology*, 152, 159-177.
- 701 Tamminga, A., C. Hugenholtz, B. Eaton & M. Lapointe, 2015. Hyperspatial Remote Sensing of
702 Channel Reach Morphology and Hydraulic Fish Habitat Using an Unmanned Aerial Vehicle
703 (Uav): A First Assessment in the Context of River Research and Management. *River Res*
704 *Appl* 31(3):379-391.
- 705 Tempfli, K., N. Kerle, G. Huurneman & L. Janssen, 2009. Principles of remote sensing, Enschede,
706 NL.

- 707 U.S. Department of the Interior & U.S. Geological Survey, 2016. Landsat Missions. In.
708 <http://landsat.usgs.gov>.
- 709 van de Koppel, J., J. C. Gascoigne, G. Theraulaz, M. Rietkerk, W. M. Mooij & P. M. J. Herman,
710 2008. Experimental Evidence for Spatial Self-Organization and Its Emergent Effects in
711 Mussel Bed Ecosystems. *Science* 322(5902):739-742.
- 712 van der Wal, D., J. van Dalen, A. Wielemaker-van den Dool, J. T. Dijkstra & T. Ysebaert, 2014.
713 Biophysical control of the intertidal benthic macroalgae revealed by high-frequency
714 multispectral camera images. *J Sea Res* 90:111-120.
- 715 Vereecken, H., J. Baetens, P. Viaene, F. Mostaert & P. Meire, 2006. Ecological management of
716 aquatic plants: effects in lowland streams. *Hydrobiologia* 570:205-210.
- 717 Verschoren, V., D. Meire, J. Schoelynck, K. Buis, K. D. Bal, P. Troch, P. Meire & S. Temmerman,
718 2016. Resistance and reconfiguration of natural flexible submerged vegetation in
719 hydrodynamic river modelling *Environ Fluid Mech* 16(1), 245-265.
- 720 Villa, P., M. Bresciani, R. Bolpagni, M. Pinaridi & C. Giardino, 2015. A rule-based approach for
721 mapping macrophyte communities using multi-temporal aquatic vegetation indices.
722 *Remote Sens Environ* 171:218-233.
- 723 Visser, F., C. Wallis & A. M. Sinnott, 2013. Optical remote sensing of submerged aquatic
724 vegetation: Opportunities for shallow clearwater streams. *Limnologica* 43(5):388-398.
- 725 Visser, F., K. Buis, V. Verschoren & J. Schoelynck, 2016. Mapping of submerged aquatic in rivers
726 from very high-resolution image data, using object-based image analysis combined with
727 expert knowledge. *Hydrobiologia*:19 doi:10.1007/s10750-016-2928-y.
- 728 Wiederkehr, J., C. Grac, M. Fabregue, B. Fontan, F. Labat, F. Le Ber & M. Tremolieres, 2015.
729 Experimental study of uncertainties on the macrophyte index (IBMR) based on species
730 identification and cover. *Ecol Indic* 50:242-250.
- 731 Wood, K. A., R. A. Stillman, R. T. Clarke, F. Daunt & M. T. O'Hare, 2012. Measuring submerged
732 macrophyte standing crop in shallow rivers: A test of methodology. *Aquat Bot* 102:28-33.

733 **Tables**

734 **Table 1:** Overview of the equations used to calculate the Manning coefficient, n ($s\ m^{-1/3}$). Eq. 2 is used to calculate the
 735 Manning coefficient, with A (m^2) cross-sectional area, Q ($m^3\ s^{-1}$) discharge, R (m) hydraulic radius, S ($m\ m^{-1}$) water
 736 level slope, for which all parameters are measured in both reaches of the study area. Eq. 3 and Eq. 4 are empirical
 737 relationships between the Manning coefficient and the vegetation cover (%) and Manning coefficient and the biomass
 738 ($g\ DW\ m^{-2}$), respectively All parameters are derived from the digital maps.

Reference	Equation	Number
Chow et al. (1956)	$n = \frac{A}{Q} * R^{2/3} * S^{1/2}$	Eq. 2
Green (2005)	$n = 0.0438 \exp(0.0200 * cover)$	Eq. 3
De Doncker et al. (2009)	$n = 0.4628 - 0.3998 \exp(-0.0047 * biomass)$	Eq. 4

739

740

741 **Table 2:** The accuracy (%) of the species identification of the image method compared to the ground survey method
 742 per month per river. The accuracy is based on species level; for each grid cell (n=396) the species is compared between
 743 the image method and the ground survey method.

Month	April	May	June	July	August	September
Zwarte Nete	100	100	66.4	59.6	84.8	93.7
Desselse Nete	100	100	100	100	97.0	100

744

745

746 **Table 3:**Percentage vegetation cover (%) estimated by the image method and the ground survey method (GS) for June,
 747 July, August and September in the Zwarte Nete.

Month	June		July		August		September	
Method	GS	Image	GS	Image	GS	Image	GS	Image
<i>C. obtusangula</i>	2.3	0.0	2.0	0.0	2.5	2.5	0.0	0.0
<i>M. spicatum</i>	-	-	-	-	-	-	-	-
<i>P. pectinatus</i>	1.3	0.0	25.5	24.0	5.1	0.0	-	-
<i>S. emersum</i>	32.3	29.6	62.1	59.3	86.4	97.5	4.6	6.1
Riparian vegetation	-	-	-	-	-	-	-	-
Bare sediment	64.1	70.4	10.4	16.6	1.0	0.0	95.5	94.0

748

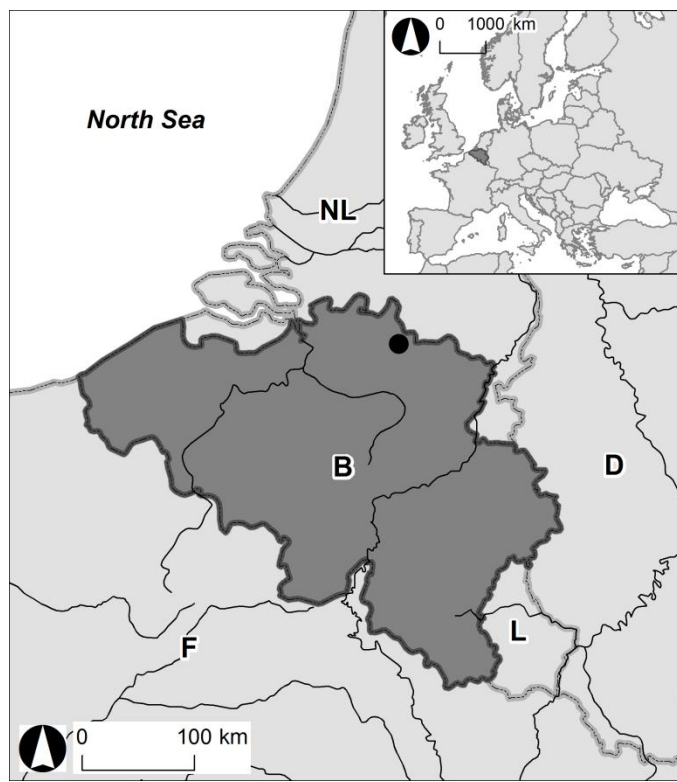
749 **Table 4:**Total biomass (gDW m⁻²) per month in both rivers. The biomass is estimated by the image analysis method
 750 and by mowing method when all vegetation was removed and weighed.

Month	April	May	June	July	August	September
Zwarte Nete						
Image	0	3.3 ± 0.1	11.4 ± 3.0	56.8 ± 5.9	187.5 ± 34.2	10.8 ± 1.3
Mowing	-	-	-	-	193.3	-
Desselse Nete						
Image	0.9	65.8 ± 8.8	101.6 ± 26.4	36.7 ± 7.9	150.4 ± 24.4	13.8 ± 3.5
Mowing	-	-	-	-	123.6	-

751

752 **Table 5:** Comparison of the current method with five other remote sensing approaches using optical imagery and ground level visual survey. The features where the
 753 current method performs good are highlighted in bold.

	Spatial resolution (pixel edge length)	Temporal resolution	Spectral region	Operation cost	Collection cost	Spatial extent	Weather dependency	Knowledge requirements (obtaining, processing)
This study	< 1 cm	Flexible	RGB	Low (man hours, consumables)	Low	m ²	Low (sun)	Low
Kite, blimp and balloon photography (Barrell and Grant 2015; Bryson et al. 2013; Guichard et al. 2000)	< 5 cm	Flexible	RGB NIR	Low (man hours, consumables)	Medium	m ²	Medium (sun, wind speed)	Medium
Unmanned aerial vehicles (Rango et al. 2010)	1-10 cm (dependent on sensor and flight height)	Flexible	RGB NIR	High (training, man hours, post-processing)	Medium	m ² - hm ²	Medium (sun, wind speed)	High
Manned aircraft imaging	0.3 - 5m (dependent on flying height)	Flexible	RGB NIR MIR	High (plane charter, post-processing)	High	m ² - km ²	High (sun, sky conditions)	High
Freely available satellite images (NASA 2016; U.S. Department of the Interior and U.S. Geological Survey 2016)	> 5 m	Fixed Several/year (dependent on location and resolution)	RGB NIR MIR	0	0	> 1 km ²	High (sun, sky conditions)	Medium
Commercial satellite images (Apollo Mapping 2016; Satellite Imaging Corporation 2016)	0.5-5 m	Fixed 14-100 days (dependent on location and resolution)	RGB NIR MIR	0	High	> 1 km ²	High (sun, sky conditions)	Medium
Ground level visual survey	Variable	Flexible	-	High	-	m ²	None	Low

755 **Figures**

756

757 **Figure 1:** The location of the study area is indicated with a black dot in the North East of Belgium. Insert: the location

758 of Belgium in Europa is shown in dark grey.

759

760

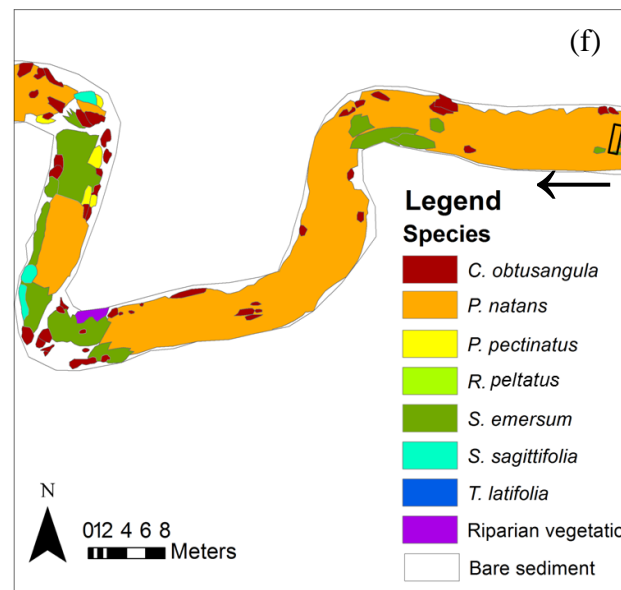
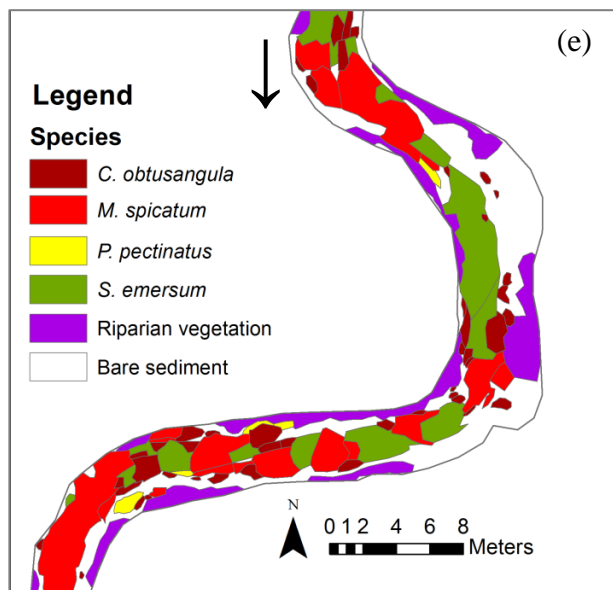
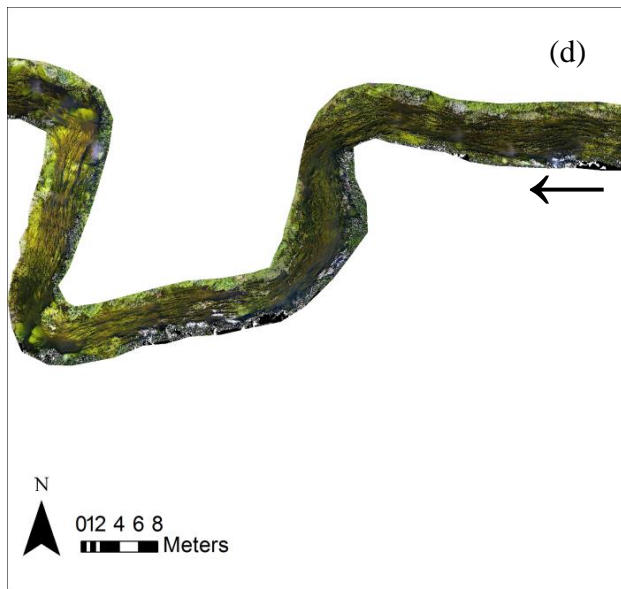
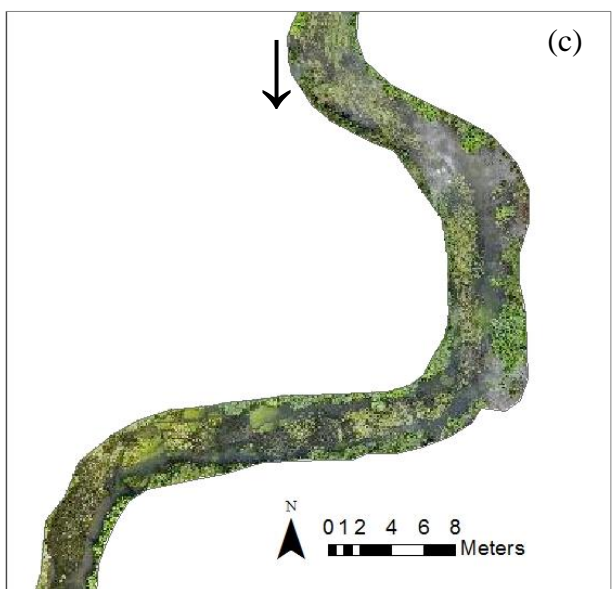
(a)



(b)

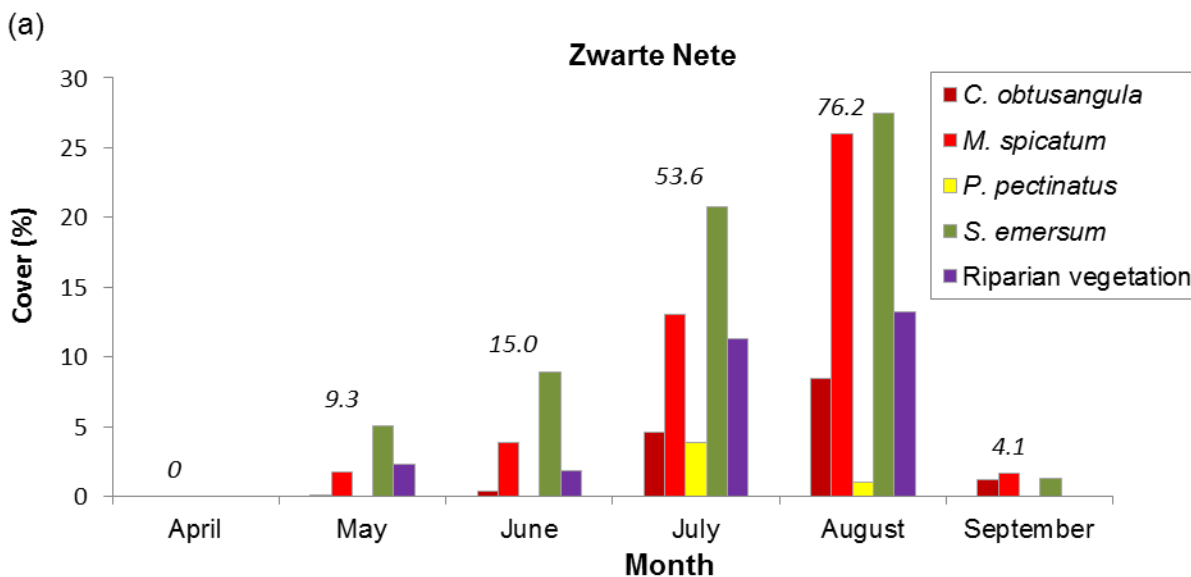
761 **Figure 2:** Illustrations of the image collection in the field. (a) The DSLR camera is attached with a ball head to a
762 handheld telescopic pole to take orthogonal images. (b) One person holds the pole with camera tilted in order to
763 position the camera at a height of 5 m above the water surface. A second person checks with a live view on a laptop
764 that both river banks are visible on each image and takes the images with tethered capture.

765

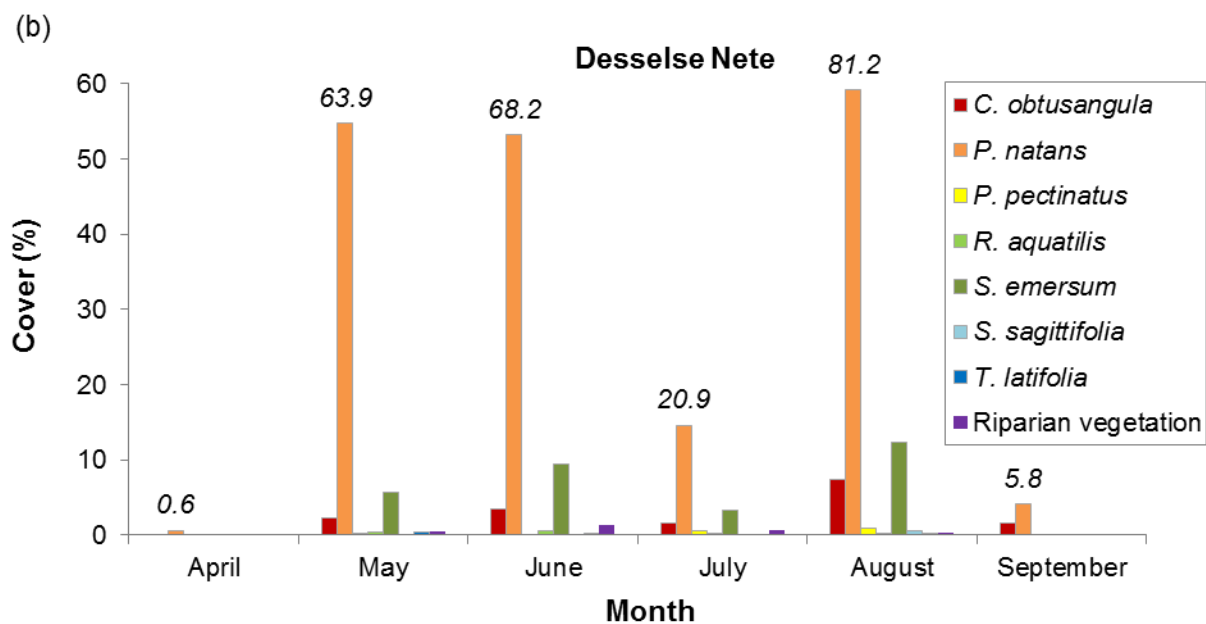


766 **Figure 3:** Examples are given of the image collection, processing and analysis in the **(a, c, e)** Zwarte Nete and the **(b,**
767 **d, e)** Desselse Nete on the 13th of August 2013. Illustrations are shown of (a, b) individual images taken with a DSLR
768 camera attached to a pole, (c, d) a plan view of a part of the image mosaic, (e, f) vegetation map with colors indicating
769 the species and the location of the ground survey (black rectangular). The water flow direction is indicated with an
770 arrow.
771

772



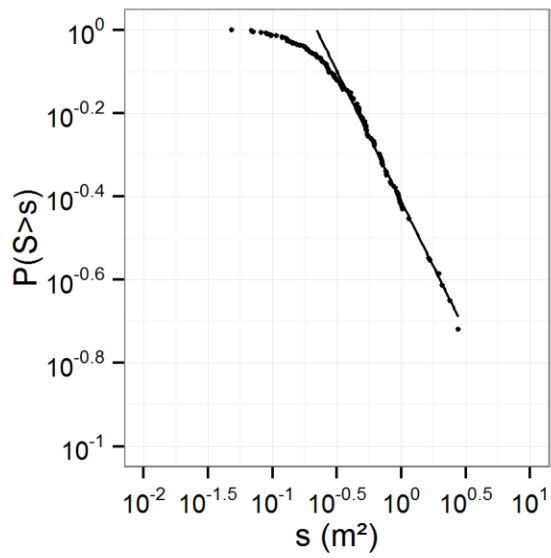
773



774

775 **Figure 4:** Vegetation cover per species per month for the reach in the (a) Zwarte Nete and (b) Desselse Nete. The
 776 colors of the bars refer to the species, the same colors for the species as in Fig. 3 are used (submerged species: red-
 777 yellow, floating species: green, emerged species: blue). The total vegetation cover per month is added in italics.

778

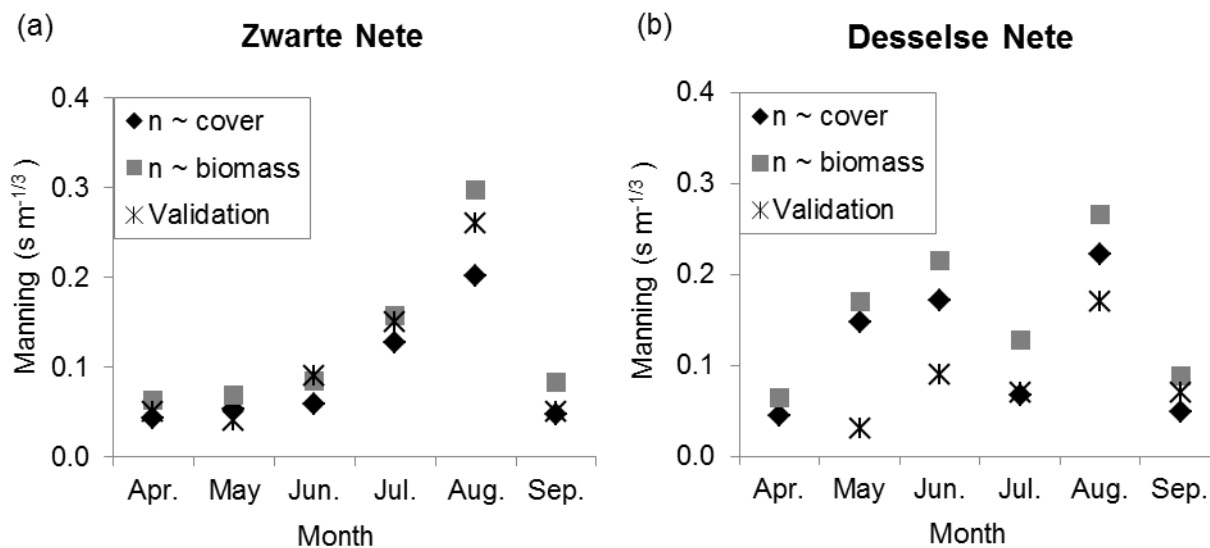


779

780 **Figure 5:** The inverse cumulative distribution of the patch sizes of *C. obtusangula* plotted on a double logarithmic
781 scale. A power-law relationship is added with $\beta = 0.6$ of Eq.1 ($p < 0.001$; $R^2 = 0.99$).

782

783



784

785 **Figure 6:** Manning coefficient in function of time for the (a) Zwarte Nete and (b) Desselse Nete. For the validation
 786 the Manning coefficient is calculated with Eq. 2(*) based on field measurements, Table 1. The Manning coefficient is
 787 calculated with Eq. 3 (■) and Eq. 4 (◆), these are empirical relationships with cross-sectional blockage and biomass,
 788 respectively see Table 1.

789

790 **Appendix**

791 **Table 6:** Overview of the measured hydraulic data per river per month. These values are used to calculate the Manning
 792 coefficient with Eq. 2.

		April	May	June	July	August	September
Zwarte Nete							
Discharge	(m ³ s ⁻¹)	0.28	0.5	0.23	0.25	0.2	0.46
Cross-sectional area	(m ²)	1.06	1.39	1.28	1.97	2.36	1.69
Hydraulic radius	(m)	0.35	0.43	0.37	0.43	0.51	0.39
Water level slope	(m m ⁻¹)	0.0007	0.0007	0.0009	0.0012	0.0013	0.0005
Desselse Nete							
Discharge	(m ³ s ⁻¹)	0.45	0.61	0.33	0.39	0.32	0.61
Cross-sectional area	(m ²)	1.43	1.63	1.76	1.90	2.65	2.32
Hydraulic radius	(m)	0.38	0.33	0.44	0.46	0.57	0.52
Water level slope	(m m ⁻¹)	-	0.0005	0.0009	0.0006	0.0009	0.0008

793

794 **Table 7:** The biomass:cover conversion factor mean \pm standard error (g m⁻²) is measured per month for *C.*
 795 *obtusangula*, *S. emersum* and *P. natans* (n=3). Note that no replicates were taken in April, so no standard error is
 796 given.

	Apr.	May	Jun.	Jul.	Aug.	Sept.
<i>C. obtusangula</i>	28.5	NA	114.8 \pm 37.7	123.7 \pm 8.6	238.4 \pm 50.3	354.9 \pm 41.0
<i>P. natans</i>	146.0	116.6 \pm 15.9	172.8 \pm 45.3	209.8 \pm 48.3	174.5 \pm 19.5	190.6 \pm 67.6
<i>S. emersum</i>	1.1	4.6 \pm 1.7	49.9 \pm 8.5	85.3 \pm 14.0	202.2 \pm 62.0	64.0 \pm 10.7

797